Untethered control of functional origami microrobots with distributed actuation

Larissa S. Novelino[a,1], Qiji Ze[b,1], Shuai Wu[b,1], Glaucio H. Paulino[a,2], and Ruike Zhao[b,2]

[a]School of Civil and Environmental Engineering, Georgia Institute of Technology, Atlanta, GA 30332; and [b]Department of Mechanical and Aerospace Engineering, The Ohio State University, Columbus, OH 43210

Edited by John A. Rogers, Northwestern University, Evanston, IL, and approved August 19, 2020 (received for review June 28, 2020)

Deployability, multifunctionality, and tunability are features that can be explored in the design space of origami engineering solutions. These features arise from the shape-changing capabilities of origami assemblies, which require effective actuation for full functionality. Current actuation strategies rely on either slow or tethered or bulky actuators (or a combination). To broaden applications of origami designs, we introduce an origami system with magnetic control. We couple the geometrical and mechanical properties of the bistable Kresling pattern with a magnetically responsive material to achieve untethered and local/distributed actuation with controllable speed, which can be as fast as a tenth of a second with instantaneous shape locking. We show how this strategy facilitates multimodal actuation of the multicell assemblies, in which any unit cell can be independently folded and deployed, allowing for on-the-fly programmability. In addition, we demonstrate how the Kresling assembly can serve as a basis for tunable physical properties and for digital computing. The magnetic origami systems are applicable to origami-inspired robots, morphing structures and devices, metamaterials, and multifunctional devices with multiphysics responses.

untethered actuation | origami | magnetic actuation | origami computing | multifunctional systems

Origami, the art of paper folding, has unfolded engineering applications in various fields. We can find such applications in materials (1, 2), electrical (3), civil (4), aerospace (5, 6), and biomedical (7) engineering. Those applications take advantage of the origami shape-changing capabilities to create tunable, deployable, and multifunctional systems. Naturally, shape-changing systems require proper actuation. Unfortunately, the lack of a robust solution for shape actuation is one of the barriers to widespread use of origami-based engineering solutions. While many applications focus on mechanical (8) and pneumatic (9–12) actuations, those solutions result in bulky assemblages with excessive wiring. Although other solutions exist, where thermo- (6, 13, 14), humidity- (15), and pH-responsive (16) materials are adopted, the actuation speed of the shape transformation is significantly limited by the slow response rate of the materials and/or actuation sources.

By means of origami engineering, kinematic shape change can be synergistically integrated with mechanical instabilities to devise functional mechanisms (12, 17–19). Such instabilities may arise from nonrigid foldable patterns with an unstable deformation path leading to a stable state, representing multistability and instantaneous shape locking (2, 10). The Kresling pattern (20) is an example of a geometrically bistable pattern that can be spontaneously generated on a thin cylindrical shell under axial and torsional load, displaying a natural coupling between axial deformation and rotation. For a bistable Kresling, the bistability represents an instantaneous shape locking of the pattern in the two stable states, which are achieved either by axial forces or torques that are superior to the energy barrier between states. When composed of axially assembled N unit cells, the Kresling assembly can effectively accomplish tremendous height shrinkage, while possessing the capability of achieving 2^N independent stable states if each unit cell is actuated locally. Because of those properties, this pattern has been used in several applications, such as metamaterials (21, 22), robots (8), and wave propagation media (23). However, under currently available actuation methods (e.g., motors, pressure, shape memory polymers, and hydrogels), those Kresling structures are limited by slow actuation or bulky wiring systems. Further, local/distributed control requires multiple actuation sources as well as multiple controllers, leading to increased system complexity.

Recently, magnetic-responsive materials have emerged as a promising alternative for shape control (24, 25), as this allows for untethered ultrafast and controlled actuation speed, as well as distributed actuation (26, 27). The magnetic untethered control separates the power source and controller out of the actuator by using field-responsive materials, making applications possible at different scales (e.g., macro, micro, and nano). These features promote magnetic actuation as an ideal solution for origami shape transformation, as explored in this paper. Thus, we attach magnetic-responsive plates to the Kresling unit cells for the application of torsion to a level that triggers the bistable state transition (Fig. 1*A*). This torsional force is instantaneously generated in the presence of an external magnetic field **B**, which causes the plate to rotate while trying to align its programmed magnetization **M** with **B**. For a multicell Kresling assembly, with a magnetic plate attached on each unit cell, different magnetic torque intensities and directions can be exerted by distinguishing

Significance

Over the past decade, origami has unfolded engineering applications leading to tunable, deployable, and multifunctional systems. Origami-inspired structures currently rely on the use of actuation methods that are pneumatic, mechanical, stimuli-responsive, etc. These actuation strategies commonly lead to bulky actuators, extra wiring, slow speed, or fail to provide a local and distributed actuation. In this work, we introduce a magnetically responsive origami system to expand its shape-changing capability for multifunctionality. We anticipate that the reported magnetic origami system is applicable beyond the bounds of this work, including robotics, morphing mechanisms, biomedical devices, and outer space structures.

Author contributions: G.H.P. and R.Z. designed research; L.S.N., Q.Z., and S.W. performed research; L.S.N., Q.Z., and S.W. contributed new reagents/analytic tools; L.S.N., Q.Z., S.W., G.H.P., and R.Z. analyzed data; and L.S.N., Q.Z., S.W., G.H.P., and R.Z. wrote the paper.

The authors declare no competing interest.

This article is a PNAS Direct Submission.

[1]L.S.N., Q.Z., and S.W. contributed equally to this work.

[2]To whom correspondence may be addressed. Email: zhao.2885@osu.edu or paulino@gatech.edu.

This article contains supporting information online at https://www.pnas.org/lookup/suppl/doi:10.1073/pnas.2013292117/-/DCSupplemental.

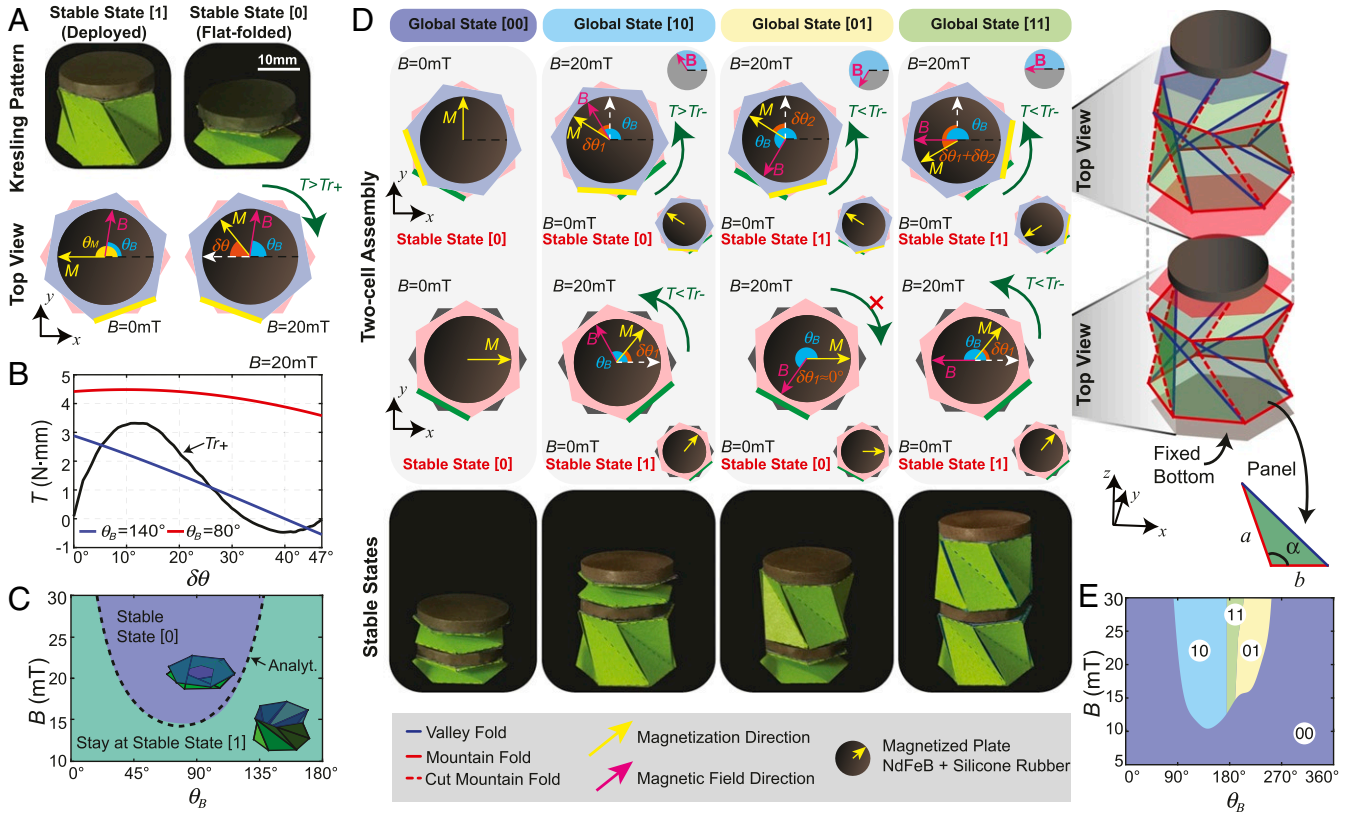

Fig. 1. Magnetic actuation of the Kresling pattern and assembly. (*A*) Kresling pattern with a magnetic plate at deployed and folded states, where θ_B is the direction of the applied magnetic field **B**, θ_M is the direction of the plate magnetization **M**, and $\delta\theta$ is the rotation angle controlled by **B**. (*B*) Torque required to fold the unit cell and magnetic torque versus plate rotation angle $\delta\theta$ at given **B**. (*C*) Contour plot of the analytical and measured results showing whether the unit cell will switch from stable state [1] to stable state [0], depending on the direction θ_B and intensity *B*. Dashed line represents the analytical prediction. (*D*) Schematics of the magnetic actuation of a two-cell Kresling assembly. The first column represents the initial state of the unit cells, and the other three columns show the three different stable states of the assembly after the magnetic actuation. The parameters $\delta\theta_1$ and $\delta\theta_2$ denote the rotation angle of the bottom and top unit cells, respectively. In each column, the corner *Insets* represent the unit cell state after the magnetic field is removed. $Tr+$ and $Tr-$ represent the required torques to fold and deploy the unit cell, respectively. The red cross (on the third column) denotes that the rotation is constrained by the geometry. (*E*) Contour plot of experimental measurements for the actuation from the [00] state to the other three states.

the magnetization directions of the magnetic plates. The unit cells can be actuated either simultaneously or independently by using different magnetic torques of the magnetic plates and distinct geometric–mechanical properties of each unit cell. Further, the magnetization directions change with the states of the multicell assembly, allowing multimodal distributed actuation by controlling just the magnetic field.

The remainder of this paper is organized as follows. First, we discuss the design and actuation of the Kresling pattern using different strategies, and the mechanical behavior with the magnetic actuation. Next, we provide two examples of applications of the magnetically actuated Kresling: 1) a Kresling assembly with tunable mechanical property and 2) a magneto-mechano-electrical Kresling pattern for digital computing. Then, we conclude with final remarks.

Results and Discussion

Geometry and Magnetic Actuation. The Kresling pattern is a nonrigid foldable origami, meaning deformation is not restricted only to folding hinges but also involves bending and stretching of both panels and hinges. This nonrigid behavior is what allows for unit cell bistability. Although, theoretically, geometrically designed Kresling unit cells present bistability, the material plays an important role in whether or not this behavior will be observed in the fabricated unit cell. Thus, to guarantee bistability, the design of the pattern parameters (panel angle α, and lengths a and b in Fig. 1*D*) is guided by both geometric relations (28) and computational mechanics simulations (29) (*SI Appendix*, section 1 and Table S1). The Kresling unit cells are fabricated with cut-relieved hinges (30); that is, we replace diagonal mountain folds by cuts (*SI Appendix*, Fig. S1). In each unit cell, we add a magnetic-responsive plate with volume V and a programmed magnetization **M**, whose direction is always in the plane of the plate. In the presence of an external magnetic field **B**, a magnetic torque $\mathbf{T} = V(\mathbf{M} \times \mathbf{B})$ is generated, which tends to align the plate magnetization direction θ_M with the magnetic field direction θ_B. Note that the direction of the applied magnetic field is also in the plane of the plate, so that the induced magnetic torque causes a rotational motion of the plate around the longitudinal axis of the Kresling unit cell. This motion twists the unit cell by an angle $\delta\theta$. Fig. 1*A* shows a single unit cell that folds under a clockwise magnetic torque (Movie S1). Because the unit cell is bistable, an energy barrier has to be overcome for the switch from stable state [1] (deployed) to state [0] (folded). We experimentally quantified this energy barrier (*SI Appendix*, sections 3 and 6) by obtaining the required torque to fold the unit cell (black curve in Fig. 1*B*). This means that the magnetic torque has to be both clockwise and larger than the required torque ($Tr+$) for the unit cell to fold. The magnetic torque T with clockwise as the positive direction is computed as $T = BMV\sin(\theta_M - \theta_B)$, where B is the magnetic field intensity, M is the magnetization intensity of the magnetic plate (*SI Appendix*, section 7), and both directions θ_B and θ_M are defined with respect to the x axis. Taking the case with magnetization direction $\theta_M = 180°$ at the

deployed state, as an example, the Kresling pattern folds when the provided magnetic torque is larger than the required torque during the entire folding process (red curve in Fig. 1*B* with $B = 20$ mT and $\theta_B = 80°$). Note that the magnetic torque varies during the rotation of the magnetic plate. If the applied magnetic torque is smaller than the required torque at any angle during the entire folding process (blue curve in Fig. 1*B* with $B = 20$ mT and $\theta_B = 140°$), the Kresling pattern will fail to achieve the folded state and will return to the deployed state when the magnetic field is removed. Because of the tunability of the magnetic field, the actuation speed can be controlled as quickly as a tenth of a second as shown in Movie S1. Fig. 1*C* shows the required actuation condition (combination of B and θ_B) to fold the Kresling from state [1] to [0] (*SI Appendix*, sections 4 and 8). For the deployment of the unit cell (switching from state [0] to [1]), a counterclockwise torque $T < Tr-$ throughout the rotation is required. *SI Appendix*, Fig. S11 shows the deployment process and required actuation condition.

Distributed Actuation. Rationally designing the individual magnetization on each unit cell of the Kresling assembly allows a distributed torque to be introduced along the longitudinal axis of the assembly and under the applied magnetic field. To explain the concept, Fig. 1 *D* and *E* shows the actuation of a two-cell assembly with equivalent geometries (*SI Appendix*, section 5). The global states are defined by a binary code [*ij*], with *i* and *j* denoting the bottom and top unit cells, respectively. For example, global state [10] corresponds to the state in which the bottom unit cell is deployed and the top unit cell is folded. Each unit cell behaves differently due to the different magnetization directions of the attached magnetic plates (e.g., 0° and 90° at the folded state [00]). By tailoring the intensity and direction of the magnetic field, the two-cell assembly can be precisely actuated from, and to, any of the four stable states. In Fig. 1*D*, we provide the top view of the unit cells as the assembly switches from the stable state [00] to the other three stable states under a 20 mT magnetic field (Movie S2). Starting from the state [00], when a 20-mT magnetic field is applied at $\theta_B = 120°$, the torque generated is enough to deploy the bottom unit cell, but not the top one, leading to a new stable state [10]. Note that the torque generated on the top unit cell is determined only by the top magnetic plate, while the torque acting on the bottom unit cell is the vector summation of the magnetic torques from both magnetic plates. Thus, only the bottom unit cell can change state, rotating by $\delta\theta_1$, making the top unit cell rotate with it by rigid body motion (i.e., $\delta\theta_2 = \delta\theta_1$). Fig. 1*E* shows the contour plot of the magnetic field direction and the intensity needed to keep the global state at [00] or to switch to any of the three other stable states [10], [11], and [01]. In *SI Appendix*, Fig. S12, we present the contour plots for the actuation starting from the stable states [10], [11], and [01], which provides guidance to achieve sequential deformations from a specific state to the others.

Based on the concept of distributed actuation, one could theoretically and ideally achieve 2^N stable states from a Kresling assembly with N unit cells. This multistable assembly therefore enables a large number of state shiftings, which can be further explored for multifunctional applications such as tunable physical properties and logic computing that will be discussed in the following sections.

State Shifting of Kresling Assembly. Taking advantage of distributed actuation, we explore the state shifting behavior of the

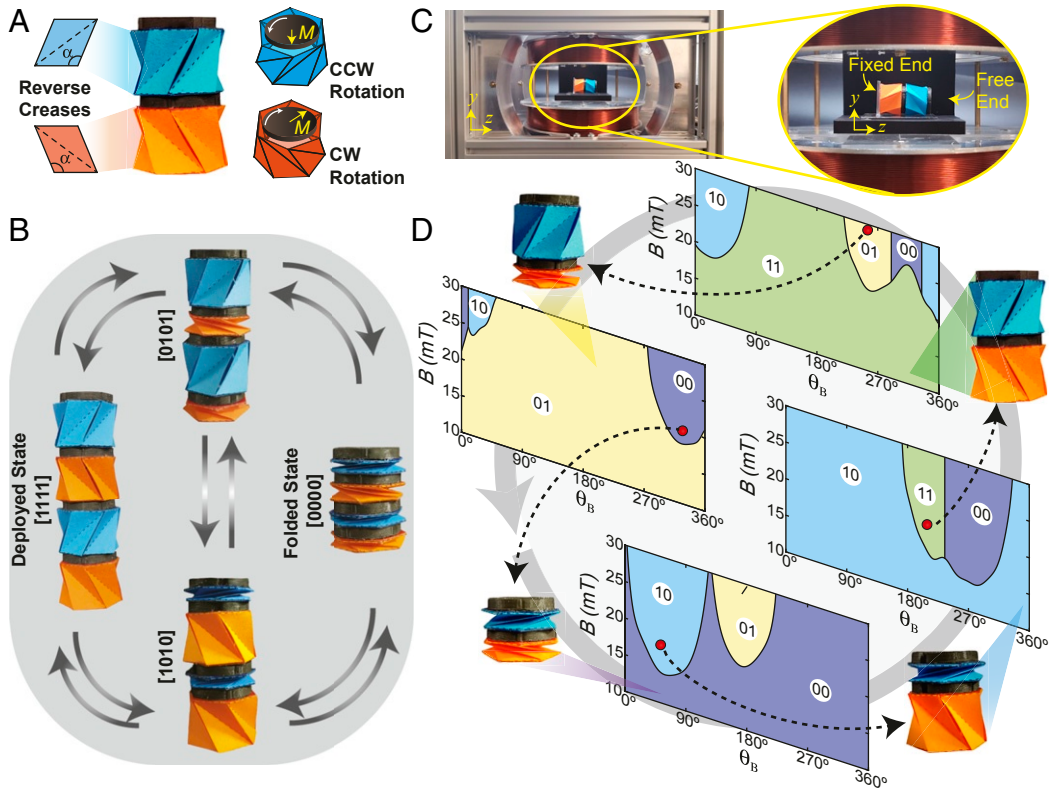

Fig. 2. Magnetic actuation of generalized reverse creases Kresling assemblies with multiple cells. (*A*) Two-cell Kresling assembly with reverse creases. (*B*) Sequential magnetic actuation of unit cells with reverse creases. (*C*) Magnetic actuation setup used to provide the 2D magnetic field. (*D*) Magnetic actuation of multicell assembly with reversed creases leading to cyclic switch of states [11], [01], [00], [10], [11], . . ., etc. Each contour plot provides the set of actuation parameters (B and θ_B) needed to switch the unit cell from one stable state to the other.

Kresling with enhanced programmability by assembling unit cells with reverse creases. As shown in Fig. 2*A*, the two assembled unit cells are chiral to each other and have opposite folding rotational direction. The orange unit cell folds under clockwise (CW) rotation, while the blue unit cell folds under counterclockwise (CCW) rotation. As an example, we show, in Fig. 2*B*, a four-cell Kresling assembly with chiral unit cells (blue–orange–blue–orange) in which we can program the actuation of the achiral groups (represented by same colors) to fold/deploy together. This strategy also allows for two global actuation modes: 1) purely rotational modes in which the change in global state occurs without axial displacement (represented by switching between states [1010] and [0101] in Fig. 2*B*) and 2) purely axial modes in which the change in global state occurs without the change in global rotation (for example, switching between states [1111] and [0000] in Fig. 2*B*). This occurs because the rotations of the pair of chiral unit cells cancel each other, leading to no rotation between the polygonal panels in the two extremities. The distributed actuation allows us to achieve the fully and selectively folded/deployed states even though we control the unit cells in groups. All of the reported actuation strategies are possible because of the local response of the magnetic plates, assembled directly on the unit cell under the two-dimensional (2D) magnetic field generated by the setup in Fig. 2*C*. The setup consists of two pairs of coils along the Cartesian x and y directions. Inside the coil assembly, the samples are attached to an acrylic base that kinematically restricts one of the ends, leaving the other end free for any type of displacement. In Fig. 2*D*, we show the contour plots with the measured actuation parameters (B and θ_B) needed to cyclically switch states [11], [01], [00], and [10] (Movie S3). Although some transformations cannot be attained directly, the actuation actually closes a loop, meaning that we can actuate the Kresling assembly to all of the possible global stable states via the ultrafast magnetic actuation method by controlling applied magnetic field intensity and direction.

Distributed Actuation for Tunable Physical Property. The aforementioned discussion focuses on the Kresling assemblies with the same unit cell geometry (same required torque and energy barrier between stable states). Since their multicell assemblies are capable of shifting between states under the distributed actuation, we geometrically engineer the energy barriers needed to fold/deploy each unit cell to achieve tunable physical property. In our designs, the polygon size and type are fixed, and only the height of the unit cell in the deployed state is changed to effectively tune the required energy barrier. From those constraints, the crease pattern parameters are computed (*SI Appendix*, section 1). The increase in height relates to the increasing of the energy barrier between states, as shown in Fig. 3 *A* and *B* by the experimentally measured force–displacement curves and the computed stored energy of the unit cells under the axial compression load (*SI Appendix*, section 3). The samples are fixed at the bottom, which restricts both rotation and axial displacement, and are completely free at the top (Fig. 3*A*). Because of the specific test boundary conditions (fixed–free ends), we do not obtain (measure) negative forces. Instead, the null forces in Fig. 3*A* indicate that the unit cell snaps and loses contact with the load cell. Although the test gives no information about the unit cell during the snapping process, it provides the height change between the states of each unit cell and the stored energy prior to snapping (Fig. 3*B*). The initial slope of the force–displacement curve

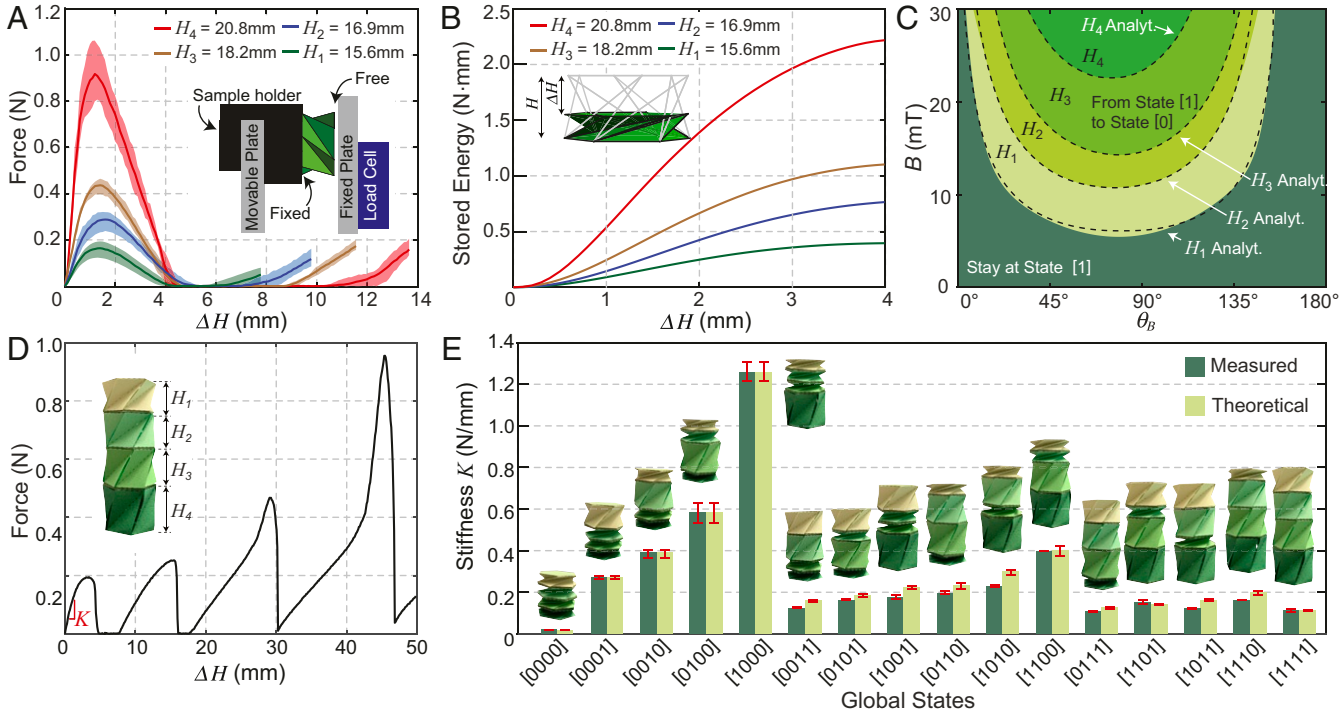

Fig. 3. Tunable mechanical response of a multicell Kresling assembly. (*A*) Measured force–displacement curves for unit cells with distinct heights. Solid lines represent the average responses, and shaded envelopes delimit maximum and minimum response ranges. *Inset* shows the schematic of the compression setup with fixed–free boundary conditions. (*B*) Stored energy versus axial displacement, obtained from the averaged force–displacement curves prior to snapping. (*C*) Contour plot with measured and analytical (dashed lines) conditions for the magnetic actuation depending on each unit cell geometry. (*D*) Measured force–displacement curve for a four-cell Kresling assembly in the stable state [1111]. (*E*) Tunable mechanical response of the four-cell Kresling assembly. From multiple consecutive testing cycles, we obtain the average (columns) and maximum/minimum (error bars) stiffness of the assembly. Theoretical values are approximated by a system of springs in series (*SI Appendix*, section 3).

can be further used to calculate the stiffness of each unit cell. From the uniaxial compression, we obtain the required torque needed to actuate each unit cell design (*SI Appendix*, section 6 and Fig. S14), which guides the parameter design of the magnetic actuation. Fig. 3*C* shows the contour plots with the analytical and experimental values for the actuation parameters. It can be seen that actuation of the unit cells with higher energy barrier requires larger B, meaning that we can use distinct energy barriers for actuation, where the wide range of magnetic field intensity allows for the local control of assemblies with a larger number of unit cells (e.g., $N > 4$).

The assembly of geometrically different unit cells enables tunable mechanical properties under the distributed magnetic actuation. Because each unit cell presents a distinct stiffness, we can conceptualize the assembly as springs in series and compute the stiffness of the system in each one of the global states, where the Kresling units are selectively folded/deployed. Fig. 3*D* shows the experimental force–displacement curve for the four-cell assembly. In this plot, we observe a sequential compression of the unit cells. In the first linear region, we characterize the stiffness K at the all-deployed state [1111]. Similarly, we characterize the stiffness of the assembly at the other states and report it in Fig. 3*E* together with the theoretical values (*SI Appendix*, section 3). From this figure, we observe that, using the proposed distributed actuation, we can tune the stiffness of the assembly by switching between stable states.

Multifunctional Origami for Digital Computing. Origami systems have recently been explored for digital computing because of the potential applications in intelligent autonomous soft robots, integrating the capabilities of actuation, sensing, and computing in the origami assemblies, acting as either basic logic gates (15) or integrated memory storage devices (22). The multifunctional origami can eliminate the requirement of conventional rigid electronic components and its stiffness mismatch with compliant origami bodies. The bistable nature of the Kresling pattern shows its potential in representing a binary system for digital computing, introducing multifunctionality into our Kresling system that goes beyond structural actuation. To develop a multifunctional Kresling assembly, we employ a magneto-mechano-electric device that incorporates actuation and computing capabilities, which could be further extended to sense external stimulation. The operation of the assembly is based on the distributed actuation of the Kresling unit cells with distinct, geometrically designed, energy barriers. By treating the applied magnetic torque as the input signal and digitizing the resultant mechanical states of the Kresling pattern as digital output [1] (deployed state) or [0] (folded state), it can be regarded as a Schmitt Trigger (Fig. 4*A*), a basic comparator circuit to convert analog input signal to a digital output signal. The higher and lower thresholds of the "Origami Schmitt Trigger" are the required torques ($Tr+$ and $Tr-$) to change the stable state of the unit cell (*SI Appendix*, section 9). In Fig. 4*A*, blue and green LEDs are used to represent the folded and deployed stable states, respectively. To construct the circuit, copper tape is attached inside the unit cell to form two switches (Fig. 4*B*): Switch 0 is connected to the blue LED in series, and switch 1 is connected to the green LED in parallel (Fig. 4*A*). Starting from the deployed state, when $T > Tr+$, the unit cell changes to the folded state [0], and both switches are closed (blue paths in Fig. 4*A*). The green LED is short-circuited, and only the blue LED is turned on (Fig. 4*C*). Now, starting from the folded state, if we apply a $T < Tr-$, the unit cell changes to the deployed state [1], both switches are open, and only the green LED is turned on

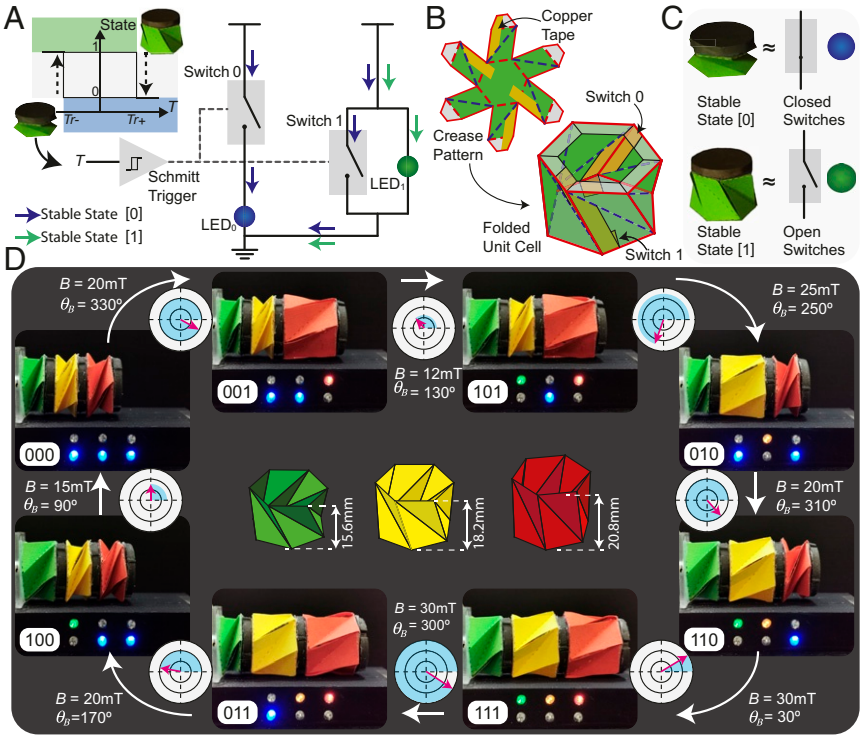

Fig. 4. Origami logic circuit with LED. (*A*) Schematics of the electric circuit of a single unit cell, where the arrows show the current direction depending on the state of the unit cell. If the unit cell is deployed, both switches are open, and the current follows the green arrows, turning on the green light. Otherwise, the switches are closed, and the blue light is on. (*B*) Schematics showing the placement of the copper tape inside the crease pattern and folded unit cell. (*C*) Schematic showing how the state of the unit cell controls whether both switches are open or closed. (*D*) Demonstration of the logic circuit on a multicell pattern with unit cells with distinct energy barriers.

(green path in Fig. 4*A*). If the applied magnetic torque is not enough to change the state of the Kresling pattern, the "Origami Schmitt Trigger" remains in its state and possesses memory. Thus, using the concept of the "Origami Schmitt Trigger," we design a device for three-bit information storage and display by a three-cell magneto-mechano-electric Kresling assembly that has three different energy barriers and controllable multimodal distributed actuation (Fig. 4*D*). Each unit cell is represented by two LEDs, with lighted blue denoting the folded state. The other colored LEDs are green, yellow, and red, whose lighted state denotes the deployed state of the unit cell with the same color. In this way, the state of the Kresling assembly is digitized as three-bit information with real-time display. Fig. 4*D* demonstrates the transition between the eight states in a loop by accurately controlling the intensity and direction of the magnetic field (B, θ_B) (Movie S4). The initial magnetization directions of the attached magnetic plates and the circuit of the Kresling assembly circuit are shown in *SI Appendix*, Table S2 and Fig. S18*C*, respectively. Note that, by designing the Kresling geometries and magnetic controlling parameters, this device can be extended to an N-layer assembly with the capabilities of N-bit information storage resulting from the 2^N distinct states. Additionally, because of the differently designed energy barriers in the assembly, the device can passively sense and actively respond to the external load, enabling an intelligent system with integrated actuation, sensing, and computing.

Concluding Remarks

This work closes the gap existing in most origami applications by providing an actuation solution that acts locally and remotely on complex origami assemblies. We propose a coupling between magnetic-responsive materials with a bistable origami pattern, eliminating the need for explicit shape-locking mechanisms, and allowing for a fast shape changing and instantaneous shape locking of those structures. In addition, we are capable of actuating complex assemblies (as opposed to single or dual unit cells) with local control. That is, each unit cell can fold and deploy independently, on demand. This approach is extendable to other origami materials, as the magnetic material is assembled to the unit cells. Thus, we envision a simple transition to other material systems, including 3D printing, previously used to fabricate origami structures.

Materials and Methods

Sample Fabrication. We fabricated each Kresling unit cell by perforating and cutting the pattern on Tant origami paper (0.1 mm thick). The Kresling pattern is modified to a flower-like shape (*SI Appendix*, Fig. S1) to accommodate the cuts along the mountain folds. After the pattern is folded, we attach the top and bottom polygons that are made of 160 g/m Canson Mi-Teintes paper (0.2 mm thick). To the top of the unit cell, we attach a 3-mm-thick magnetized plate that is made from a mix of Ecoflex 00-30 silicone rubber and NdFeB (neodymium–iron–boron) particles (30 vol%). The geometry of the unit cells and magnetization directions of the plates are provided in *SI Appendix*, Tables S1 and S2. More details are provided in *SI Appendix*, section 2.

Data Availability. All study data are included in the article and *SI Appendix*.

ACKNOWLEDGMENTS. G.H.P. and L.S.N. acknowledge support from NSF Award CMMI-1538830 and the endowment provided by the Raymond Allen Jones Chair at the Georgia Institute of Technology. L.S.N. acknowledges support from the Brazilian National Council for Scientific and Technological Development, Project 235104/2014-0. R.Z., Q.Z., and S.W. acknowledge support from NSF Career Award CMMI-1943070 and NSF Award CMMI-1939543.

1. M. Schenk, S. D. Guest, Geometry of Miura-folded metamaterials. *Proc. Natl. Acad. Sci. U.S.A.* **110**, 3276–3281 (2013).
2. J. L. Silverberg *et al.*, Using origami design principles to fold reprogrammable mechanical metamaterials. *Science* **345**, 647–650 (2014).
3. S. A. Nauroze, L. S. Novelino, M. M. Tentzeris, G. H. Paulino, Continuous-range tunable multilayer frequency-selective surfaces using origami and inkjet printing. *Proc. Natl. Acad. Sci. U.S.A.* **115**, 13210–13215 (2018).
4. E. T. Filipov, T. Tachi, G. H. Paulino, Origami tubes assembled into stiff, yet reconfigurable structures and metamaterials. *Proc. Natl. Acad. Sci. U.S.A.* **112**, 12321–12326 (2015).
5. S. A. Zirbel *et al.*, Accommodating thickness in origami-based deployable arrays. *J. Mech. Des.* **135**, 111005 (2013).
6. T. Chen, O. R. Bilal, R. Lang, C. Daraio, K. Shea, Autonomous deployment of a solar panel using elastic origami and distributed shape-memory-polymer actuators. *Phys. Rev. Applied* **11**, 064069 (2019).
7. S. Li, D. M. Vogt, D. Rus, R. J. Wood, Fluid-driven origami-inspired artificial muscles. *Proc. Natl. Acad. Sci. U.S.A.* **114**, 13132–13137 (2017).
8. P. Bhovad, J. Kaufmann, S. Li, Peristaltic locomotion without digital controllers: Exploiting multi-stability in origami to coordinate robotic motion. *Extreme Mech. Lett.* **32**, 100552 (2019).
9. J. T. Overvelde *et al.*, A three-dimensional actuated origami-inspired transformable metamaterial with multiple degrees of freedom. *Nat. Commun.* **7**, 10929 (2016).
10. J. A. Faber, A. F. Arrieta, A. R. Studart, Bioinspired spring origami. *Science* **359**, 1386–1391 (2018).
11. W. Kim *et al.*, Bioinspired dual-morphing stretchable origami. *Sci. Robot.* **4**, eaay3493 (2019).
12. Y. Tang *et al.*, Leveraging elastic instabilities for amplified performance: Spine-inspired high-speed and high-force soft robots. *Sci. Adv.* **6**, eaaz6912 (2020).
13. K. Liu, J. Wu, G. H. Paulino, H. J. Qi, Programmable deployment of tensegrity structures by stimulus-responsive polymers. *Sci. Rep.* **7**, 1–8 (2017).
14. J. H. Na *et al.*, Programming reversibly self-folding origami with micropatterned photo-crosslinkable polymer trilayers. *Adv. Mater.* **27**, 79–85 (2015).
15. B. Treml, A. Gillman, P. Buskohl, R. Vaia, Origami mechanologic. *Proc. Natl. Acad. Sci. U.S.A.* **115**, 6916–6921 (2018).
16. M. Z. Miskin *et al.*, Graphene-based bimorphs for micron-sized, autonomous origami machines. *Proc. Natl. Acad. Sci. U.S.A.* **115**, 466–470 (2018).
17. P. M. Reis, A perspective on the revival of structural (In)stability with novel opportunities for function: From buckliphobia to buckliphilia. *J. Appl. Mech.* **82**, 111001 (2015).
18. A. Rafsanjani, Y. Zhang, B. Liu, S. M. Rubinstein, K. Bertoldi, Kirigami skins make a simple soft actuator crawl. *Sci. Robotics* **3**, eaar7555 (2018).
19. Y. Zhang *et al.*, A mechanically driven form of kirigami as a route to 3D mesostructures in micro/nanomembranes. *Proc. Natl. Acad. Sci. U.S.A.* **112**, 11757–11764 (2015).
20. B. Kresling, "Folded tubes as compared to kikko ("Tortoise-Shell") bamboo" in *Origami$_3$: Proceedings of the Third International Meeting of Origami Science, Mathematics, and Education*, T. C. Hull, Ed. (A.K. Peters, 2002), p. 197.
21. Z. Zhai, Y. Wang, H. Jiang, Origami-inspired, on-demand deployable and collapsible mechanical metamaterials with tunable stiffness. *Proc. Natl. Acad. Sci. U.S.A.* **115**, 2032–2037 (2018).
22. H. Yasuda, T. Tachi, M. Lee, J. Yang, Origami-based tunable truss structures for non-volatile mechanical memory operation. *Nat. Commun.* **8**, 1–7 (2017).
23. H. Yasuda *et al.*, Origami-based impact mitigation via rarefaction solitary wave creation. *Sci. Adv.* **5**, eaau2835 (2019).
24. J. Cui *et al.*, Nanomagnetic encoding of shape-morphing micromachines. *Nature* **575**, 164–168 (2019).
25. G. Z. Lum *et al.*, Shape-programmable magnetic soft matter. *Proc. Natl. Acad. Sci. U.S.A.* **113**, E6007–E6015 (2016).
26. S. Wu *et al.*, Symmetry-breaking actuation mechanism for soft robotics and active metamaterials. *ACS Appl. Mater. Interfaces* **11**, 41649–41658 (2019).
27. Q. Ze *et al.*, Magnetic shape memory polymers with integrated multifunctional shape manipulation. *Adv. Mater.* **32**, 1906657 (2020).
28. R. J. Lang, *Twists, Tilings, and Tessellations: Mathematical Methods for Geometric Origami* (CRC, 2017).
29. K. Liu, G. H. Paulino, Nonlinear mechanics of non-rigid origami: An efficient computational approach. *Proc. Math. Phys. Eng. Sci.* **473**, 20170348 (2017).
30. N. Nayakanti, S. H. Tawfick, A. J. Hart, Twist-coupled kirigami cells and mechanisms. *Extreme Mech. Lett.* **21**, 17–24 (2018).